DTU Library

^{135}La as an auger-electron emitter for targeted internal radiotherapy

Fonslet, Jesper; Lee, Boon Quan; Tran, Thuy A.; Siragusa, Mattia; Jensen, Mikael; Kibedi, Tibor; Stuchbery, Andrew E.; Severin, Gregory

[Link back to DTU Orbit](#)

IPEM Institute of Physics and
Engineering in Medicine

^{135}La as an auger-electron emitter for targeted internal radiotherapy

^{135}La as an Auger-electron emitter for targeted internal radiotherapy

J. Fonslet[1], B.Q. Lee[2,3], T.A. Tran[4], M. Siragusa[1], M. Jensen[1], T. Kibédi[3], A.E. Stuchbery[3], G.W. Severin[1,5,6*]

[1]*Hevesy Laboratory, Center for Nuclear Technologies, Technical University of Denmark, Roskilde, Denmark*

[2]*Department of Oncology, Oxford University, Oxford, United Kingdom*

[3]*Department of Nuclear Physics, Australia National University, Canberra, Australia*

[4]*Lund University Bioimaging Center, Lund University, Lund, Sweden*

[5]*Department of Chemistry, Michigan State University, East Lansing, MI, USA*

[6]*Facility for Rare Isotope Beams, Michigan State University, East Lansing, MI, USA*

Abstract:

Introduction: ^{135}La has favorable nuclear and chemical properties for Auger-based targeted internal radiotherapy. Here we present detailed investigations of the production, emissions, and dosimetry related to ^{135}La therapy.

Methods and Results: ^{135}La was produced by 16.5 MeV proton irradiation of metallic ^{nat}Ba on a medical cyclotron, and was isolated and purified by trap-and-release on weak cation-exchange resin. The average production rate was 407 ± 19 MBq/μA (saturation activity), and the radionuclidic purity was 98% at 20 h post irradiation. Chemical separation recovered > 98 % of the ^{135}La with an effective molar activity of 70 ± 20 GBq/μmol. To better assess cellular and organ dosimetry of this nuclide, we have calculated the X-ray and Auger emission spectra using a Monte Carlo model accounting for effects of multiple vacancies during the Auger cascade. The generated Auger spectrum was used to calculate cellular S-factors.

Conclusion: ^{135}La was produced with high specific activity, reactivity, radionuclidic purity, and yield. The emission spectrum and the dosimetry are favorable for internal radionuclide therapy.

Keywords: lanthanum-135, La-135, radiolanthanide, auger therapy, targeted radionuclide therapy, radionuclide production

---

* gwseverin@chemistry.msu.edu – corresponding author

1　**Introduction:**

2　The development of targeted internal radiotherapy for cancer and patient specific treatment requires

3　radionuclides with suitable half-lives, chemical properties and emissions. Several nuclides are already in

4　clinical use, notably the beta emitters ^{177}Lu and [90]Y [1,2]. In addition, preclinical studies with other

5　lanthanides, especially the terbium isotopes [149, 151, 155, 161]Tb show promise, providing a matched set of

6　isotopes with diagnostic positrons and therapeutic alpha- and beta-particles, as well as Auger electrons

7　[3–6]. The radioactive isotopes of lanthanum are chemically similar to the other lanthanides, and one in

8　particular, [135]La has potential as a therapeutic Auger electron emitter.

9

10　Auger electron emitters are particularly interesting because they have the capability to deliver radiation

11　dose to individual targeted cells while sparing surrounding tissues. This is in contrast to more commonly-

12　used therapeutic nuclides, like ^{177}Lu and ^{90}Y, which have beta emissions that traverse many cell lengths,

13　with dispersed energy deposition. The very low energy and multiplicity of Auger electrons may prove

14　useful in targeted therapy, especially in the treatment of diffuse and disseminated disease, where other

15　nuclear emissions do not allow adequate dose to the targeted cell due to excessive particle range. Further,

16　there is mounting evidence that the relative biological effectiveness (RBE) of multiple low energy

17　electrons (<10 keV) significantly exceeds that of photons and higher energy beta particles [7]. In some

18　cases the biological effect of absorbed dose from Auger electrons is 2-10 times higher than X-rays of the

19　same energy, meaning that these emissions are more potent in introducing radiation damage to living cells

20　[8–10]. Therefore, coupling Auger emitting radionuclides like [135]La with highly specific targeting vectors,

21　particularly cell-nucleus targeting moieties, has potential as a powerful therapeutic tool.

22

23　[135]La decays by electron capture (EC), primarily (>98%) to the ground state of stable [135]Ba, with a half-

24　life of 18.9 hour [11] (Figure 1). Following the decay Auger electrons are emitted which are potentially

25　useful for internal radiotherapy. Throughout this paper we use the term "Auger electrons" as designation

26　for all Auger cascade electrons, including the Coster-Kronig and Super-Coster-Kronig electrons. X-rays

27　accompany the Auger cascade with a spectrum sufficient for Single Photon Emission Computed

28　Tomography (SPECT) imaging capabilities. In small-animal studies this allows for concurrent SPECT

29　imaging, facilitating dosimetry calculations in small-animal models [12]. In the projected future human

30　use of therapeutic doses, the activity could be high enough to allow whole-body SPECT based on the low

31　abundance (1.5% branch) 480.5 keV gamma emissions.
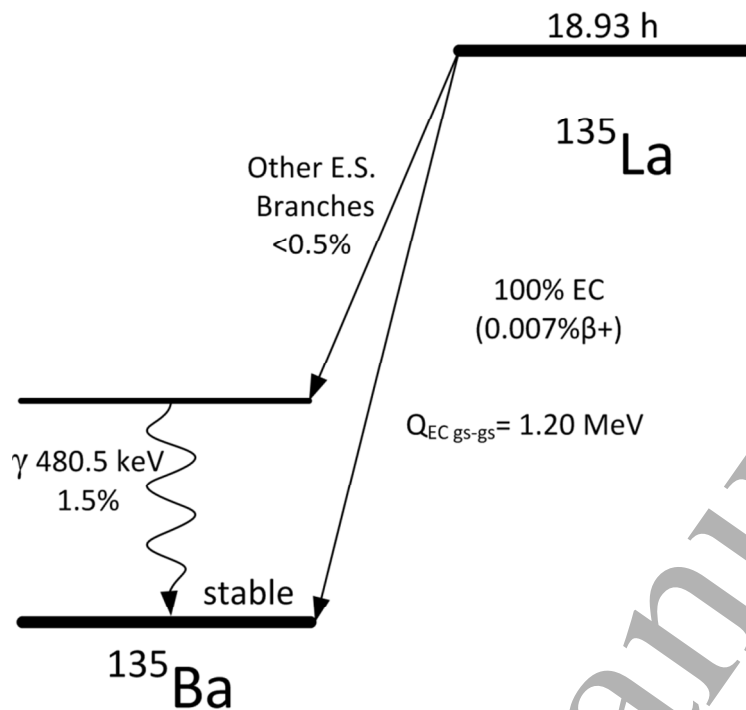
Figure 1 Simplified decay scheme of ^{135}La[11,13]**.**

When considering employing ^{135}La as a radiotherapeutic nuclide, it is necessary to make detailed dose calculations. This is important not only on the organ level, but also on the cellular level, due to the highly localized dose deposition from emitted Auger electrons. In order to get a realistic dose estimate the entire emission spectrum needs to be well understood. The conventionally-used databases (like NuDat 2 [14]) only give a condensed version of the Auger cascade emissions, without addressing the many electrons below 3 keV. Lee et al. recently developed an Auger-cascade model, BrIccEmis, based on a Monte Carlo technique for determining X-ray and Auger emission spectra [15,16]. For the present work, the model was used to obtain detailed radiation spectra from ^{135}La, especially for very low-energy Auger electrons and X-rays. Prescher et al. [17], and Tárkányi et al. [18] determined the production cross-sections for ^{135}La during proton irradiation of ^{nat}Ba at energies ranging from 12-70 MeV. Evident in their data is the fact that ^{135}La is the primary radionuclide with half-life longer than a few minutes produced in the proton-induced reactions on natural barium at energies available on most medical cyclotrons.

In this work, we detail the properties of ^{135}La as a radiotherapeutic nuclide. The practical considerations of production, purification, and radiolabeling are experimentally determined and optimized for the chelator DTPA (diethyeneltriaminepentacetic acid). Additionally, reevaluations of the Auger and X-ray

51   emission spectra are presented along with a calculation of the cellular *S*-factors and a dosimetry

52   comparison to the commonly used radiotherapeutic isotopes ^{177}Lu and [90]Y.

53

54   **Materials and Methods:**

55   *General*

56   All reagents were obtained from Sigma Aldrich and used without further purification unless otherwise

57   noted. All water was 18 MΩ MilliQ-grade (Sartorious). Hydrochloric acid (HCl) solutions were diluted

58   from 37% aq. HCl (Fluka TraceSelect) with water. pH was determined by pH paper (PEHANON 1-12

59   and 4-9). Gamma spectroscopy was performed on a Princeton Gammatech LGC 5 germanium detector,

60   calibrated using certified [133]Ba and [152]Eu sources.

61

62   *Cyclotron Production of [135]La from [nat]Ba*

63   Chunks of dendritically distilled metallic barium (99.99% trace metal grade) totaling 314-550 mg were

64   pressed with a hydraulic press (20 kN/cm^2) into a 9 mm diameter x 3 mm deep divot in a 28 mm diameter

65   x 5 mm thick silver disc. The barium was immediately covered with either 100 μm aluminum or 25 μm

66   niobium foil to reduce the exposure to atmospheric oxygen, and placed into a target holder supplying

67   direct water cooling to the backside of the silver. A rough schematic of the target and target holder can be

68   seen in a paper by Severin et al. [19]. The target holder was mounted onto a PETtrace cyclotron (PT800

69   General Electric) and irradiated at 90° (normal) incidence with 16.5 MeV protons at 15 μA for 235-280

70   min. Owing to the co-production of short-lived [134]La ($t_{1/2}$ = 6.5 min) and [136]La ($t_{1/2}$ = 9.9 min), and slightly

71   longer-lived [132]La ($t_{1/2}$ = 4.5 h) and [133]La ($t_{1/2}$ = 3.9 h), the targets were allowed to decay for 12-24 hours

72   before further handling.

73

74   In order to determine the production rates of [135]La and the other longer-lived co-produced radioisotopes

75   ([132]La, [133]La and [135m]Ba), a single thick target of Ba totaling 472 mg was irradiated at 30 μA for 227

76   minutes. This target was dissolved 19.8 hours post irradiation in 5 mL 1.2 M HCl, transferred to a plastic

77   vial, and the radionuclidic contents were quantified by gamma spectroscopy.

78

79   *Purification of [135]La*

80   The cover foil was removed and the silver disc mounted in a dissolution chamber allowing the barium to

81   be dissolved with 2 mL 4 M aq. HCl. After complete dissolution of the [nat]Ba, the solution was transferred

82   to a vial along with 1-2 mL of water to rinse. Adding the water also served to dissolve any additional

83   white precipitate present after oxidation of Ba in HCl/water. Therefore, concentrated HCl was added to

84   the dissolved target to bring the HCl concentration to 1 M acidity in a final volume of 4 mL. The solution

85   was then heated at 70 °C for at least 30 min. The pH was adjusted to ~6 with 5 mL HEPES buffer (4-(2-

86   hydroxyethyl)-1-piperazineethanesulfonic acid) (1 M, pH = 7.3, HCl/NaOH adj.) and NaOH (1 M) and

87   passed over 100 mg CM resin (Waters *Accell* Plus *CM* weak cation exchange resin) packed in a 4 mm

88   inner diameter column with polyethylene frits in order to trap the ^{135}La. The CM resin had been prepped

89   by sequential washing with 5 mL acetonitrile, 5 mL 0.1 M HCl, 10 mL water, and 3 mL 1 M HEPES pH

90   7.3. After trapping the ^{135}La, the resin was washed with 25 mL of water. Finally, the column was eluted

91   with 1 mL 0.1 M HCl to obtain the purified ^{135}La.

92

93   *Specific activity measurements*

94   Analysis by ICP-OES (inductively coupled plasma optical emission spectroscopy) was performed on the

95   samples to determine the non-radioactive, competitive metal content. The trace metals were quantified

96   using a ThermoScientific iCAP 6000 Series instrument with iTeva software. The spectrometer was

97   calibrated against standard solutions containing La, Ba, Cr, Mn, Co, Fe, Zn and Cu, which were prepared

98   by dissolution and dilution of chloride salts of the tested metals in 0.3 M HCl. Samples for analysis were

99   likewise diluted in 0.3 M HCl.

100

101   The effective molar activity was determined experimentally *via* titration of the purified ^{135}La with DTPA.

102   DTPA solutions were prepared in water by serial dilution to make concentrations spanning 8-5000 nM.

103   From these, 400 µL of each concentration was moved to an Eppendorf tube and buffered by addition of

104   100 µL of HEPES (1 M, pH = 7.4). The molar amount of DTPA used in the titration ranged 3.2-2000

105   pmol in 5 steps. To each of these Eppendorf tubes, 10 µL of 0.1 M HCl containing 3.5-4.5 MBq of ^{135}La

106   was added bringing the final pH to ~7 measured on pH paper. The titrations were performed in duplicate

107   for each separation (n = 3) with one reacting at room temperature and the other reacting at 70 °C. After 30

108   minutes, the reactions were analyzed by thin-layer chromatography (TLC) performed on aluminum-

109   backed silica (Merck TLC silica gel 60 F254), eluted with 5% (w/v) ammonium acetate in a 1:1 mixture

110   of methanol and water. In this system La-DTPA moves with the eluent, while un-chelated La^{3+} remained

111   at the origin. TLC plates were analyzed by autoradiography on a Cyclone Plus Storage Phosphor Scanner

112   (PerkinElmer) and data analysis was performed using OptiQuant software (PerkinElmer). The reaction

113   showing the chelation ratio closest to 50% was used to determine the amount of DTPA needed to chelate

114   100% of the added activity and thus the effective specific activity.

115

116   *X-ray and Auger emission spectra*

117   The initial-vacancy distribution and the energy spectra of X-rays and Auger electrons following the

118   decays of isolated ^{135}La atoms were calculated according to the methodology presented by Lee et al. [16]

119   with 10^5 Monte Carlo simulated decays. Both the condensed phase and isolated atom models were used

120   for determining the cascade distributions.

121

122   *Dosimetry*

123

124   On a cellular scale, dosimetry was treated in two ways: first by use of MIRDCell, a formalism developed

125   by MIRD (Medical Internal Radiation Dose) for calculation of cellular S-values [20,21]; and second by

126   the COOLER code [22]. The S-value is defined as the absorbed dose in the target structure from a

127   radioactive decay in the source structure, typically given in the unit Gy/(Bq·s) and denoted as S(Target←

128   Source). In this case, the target was taken to be the cell nucleus. Contributions to the nucleus (N) from the

129   nucleus (N), S(N←N), from the cytoplasm (Cy), S(N←Cy), and from the cell surface (CS), S(N←CS),

130   were separately determined. In this work, we performed MIRD-based calculations, totally within the

131   MIRD framework by taking the individual electron branches (Table 2), evaluating them in MIRDCell,

132   and then summing the doses over all emissions [20]. MIRDCell was also used to calculate the cellular

133   dosimetry of ^{177}Lu and ^{90}Y. This gave the MIRD cellular S-values as proxies for the cellular dosimetry for

134   all three isotopes (depending on the target size and source distribution). For the calculations we chose a

135   cell radius of 7 μm and nucleus radius of 5 μm. This allowed comparison with the COOLER formalism

136   (the COOLER V79 cell setting has radii of 7.1 and 5.2 μm, respectively). COOLER is a new cellular

137   dosimetry approach that uses Monte-Carlo derived stopping powers (based on PARTRAC simulations

138   [23]). This is in contrast to MIRDCell which uses Cole's electron ranges to derive an electron stopping

139   power [22,24]. The Monte-Carlo derived stopping powers generally result in altered dose distributions,

140   especially for electrons with energies in the range of 5-35 keV, coinciding with the important Auger

141   branches of the lanthanides.

142

143   In order to predict how a heterogeneously targeted tumor of macroscopic dimensions would receive dose

144   across many cell diameters, electron dose kernels were calculated in two different ways. First, by taking

145   the full electron emission spectrum (including Augers, nuclear beta emissions, and conversion electrons

146   [13,14,25]) and folding it with the range-versus-energy relationship from Cole. The dose-point kernel was

147   calculated in MATLAB for ^{135}La, ^{177}Lu and ^{90}Y. The calculation was performed using a step-size of 0.2

148   μm. Second, the electron dose-point kernel of ^{135}La was also calculated using the COOLER formalism.

149   **Results:**

150   *Cyclotron Production of ^{135}La from ^{nat}Ba*

151 When pressing the barium into the target holder, it was important to move quickly to limit the exposure of

152 the barium to air. Within the minimal (~1 minute) pressing time, a white film was observed to form over

153 the normally shiny barium. The pressed target appeared smooth, and likely had very limited surface area

154 after pressing, as compared to the dendritic chunks. In most experiments, no discoloration or alteration of

155 the target surface was observed after irradiation at a target current of 15 µA. Both aluminum (100 µm)

156 and niobium (25 µm) were tested as front foil materials, and we did not observe any qualitative difference

157 in target behavior between the two.

158

159 The end-of-saturation bombardment (EOSB) yields for the nuclides ($t_{1/2} > 3$ h) produced during proton

160 irradiation of ^{nat}Ba at 15.8 MeV (after degradation in the aluminum cover foil) are given in Table 1.

161

nuclide	$t_{1/2}$ (h)	EOSB (MBq/µA)
^{135}La	18.9	429
^{135m}Ba	28.8	4
^{133}La	3.9	29
* ^{132}La	4.6	5

162

163 **Table 1: Thick target EOSB yields for proton irradiation of ^{nat}Ba. Only nuclides with $t_{1/2}$ > 3 h are listed. *) ^{132}La is produced**
164 **both directly and via decay of the co-produced ^{132m}La isomer. The number presented here reflects the amount of ^{132}La**
165 **produced in total after all ^{132m}La has decayed to the ground state. Half-lives were obtained from refs: [11,13,26].**

166 Shorter irradiations produced a proportionately larger amount of the short-lived impurities. These short-

167 lived impurities will, at longer irradiation times, approach saturation and constitute a smaller proportion

168 of the total radioactivity. Therefore the radionuclidic purity of ^{135}La (with respect to the decay rate of the

169 other lanthanum isotopes) increases with irradiation time as long as the ^{135m}Ba impurity is chemically

170 removed.

171

172 *Target dissolution and purification of ^{135}La on Accell Plus CM resin*

173 Dissolution of the irradiated ^{nat}Ba was always rapid (3-5 min) in the HCl solution. The trapping efficiency

174 of ^{135}La on the small column of CM resin was >99%. Several loading conditions were tested: with or

175 without the 30 minute heating step, and both ammonium acetate and HEPES buffers were tested: each at

176 pH 4 and 6. It was observed that the 30-minute heating at 70 °C greatly improved trapping. When

177 omitting this step loading efficiencies of only 50% were observed. Additionally, by re-acidifying and

178 heating any washed-through solution it was possible to retain all previously untrapped activity on a

179 second column (further illustrating the importance of heating). When comparing the two buffers,

180 ammonium acetate and HEPES, it was found that HEPES at pH = 6 resulted in higher trapping efficiency.

181 The 0.1 M hydrochloric acid elution (1 mL) was >99% efficient at releasing the [135]La.

182

183 *Chemical purity and molar activity measurements*

184 ICP-OES analysis revealed the concentration of metal contaminants in the final elution. Barium was still

185 present at a concentration of 3.68 ± 0.09 µg/MBq. Cr, Mn and Fe were measured in concentrations of

186 1.64 ± 1.05 ng/MBq, 1.19 ± 0.81 ng/MBq and 1.57 ± 0.33 ng/MBq, respectively. Using the final barium

187 concentration, the separation factor was 138 ± 36. In principle, the barium removal could also have been

188 verified by the absence of coproduced [135m]Ba, as this isotope is not formed by the decay of [135]La.

189 However, the sensitivity and specificity of the gamma spectroscopy was not sufficient to detect the

190 remaining low level of barium.

191

192 The molar activity of [135]La determined by stable lanthanum assay on ICP-OES was over-optimistic for the

193 expected labelling efficiency. This is because any other lanthanide, or similar hard metal ion impurity,

194 could compete for labelling positions on vectors. Instead, the effective molar activity was assessed by

195 thin-layer chromatography analysis of DTPA titrations. In all cases, a small amount (10-15%) of [135]La

196 remained at the origin of the TLC sheet no matter how large the excess of DTPA. This was believed to be

197 due to formation of an inert lanthanum complex in the labeling solution, but the exact nature of the

198 immobile [135]La was not determined. Assuming 10% of the [135]La was thermodynamically unavailable, the

199 DTPA titrations showed an effective molar activity of 70.4 ± 20.0 GBq/µmol.

200

201 *X-ray and Auger emission spectra*

202 The initial-vacancy distribution for [135]Ba following the electron capture (EC) and internal conversion (IC)

203 processes was calculated, and as expected >99.9% of the initial vacancies created in atomic shells were

204 due to EC. The resulting total K vacancy probability was 84.9% and the total L vacancy probability was

205 11.9%. Internal conversion and electron capture processes in higher shells constituted the remaining 3.2%

206 of vacancies.

207 The calculated X-ray and Auger spectra following the decay of [135]La in the condensed-phase

208 approximation are shown in figure 2. The Auger-cascade simulations give only a small difference in the

209 resulting Auger branching ratios between the condensed-phase (with continuous filling of the outermost

210 vacancies) and isolated-atom approximations. The dose-point kernels derived from the two

211 approximations were found to slightly differ from each other only in the first 100 nm [27]. For the

212 purpose of dosimetry and possible therapeutic use, the effect is negligible and the condensed phase
213 spectra were used for dosimetry calculations.
214
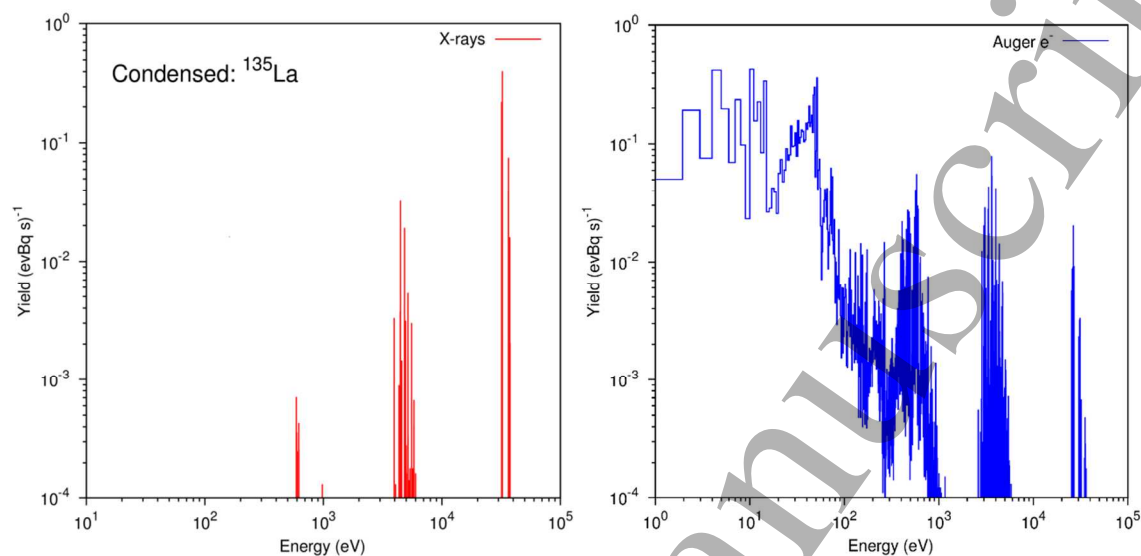
215
216 **Figure 2 Histograms (bin-size 1 eV) showing the X-ray (red) and Auger (blue) kinetic energy spectra following the decay**
217 **of ^{135}La atoms in the condensed-phase approximation of BrIccEmis. These results are tabulated in Table 2.**
218

219 Yields per decay and mean energies of the main groups of Auger electrons are summarized in Table 2.
220 The BrIccEmis derived spectrum is shown in Figure 2. Total energies released through X-rays and Auger
221 electrons per decay, are 25.8 and 6.45 keV, respectively. There are on average 10.6 Auger electrons per
222 decay (>97% of total) that have energies less than 4 keV. The maximum range of these very low-energy
223 electrons is <0.5 μm in water [28].
224
225
226
227

	Yield /decay	Mean energy (keV)
Auger KLL	0.055	26.3
Auger KLX	0.025	31.0
Auger KXY	0.003	35.6
CK LLX	0.131	0.333
Auger LMM	0.580	3.53
Auger LMX	0.185	4.33

Auger LXY	0.014	5.15
CK MMX	0.634	0.104
Auger MXY	1.59	0.538
Super-CK NNN	0.277	0.007
CK NNX	1.33	0.049
Auger NXY	4.27	0.039
CK OOX	1.78	0.009
Auger OXY	0.023	0.030
Total	10.9	0.592

228 **Table 2: Auger average spectrum following ^{135}La decay, the standard deviation in the total number of electrons ejected per**
229 **decay is 3.2 e$^-$/(Bq s).**

230

X-ray	Yield /decay	Mean energy (keV)
Kα_1	0.404	32.3
Kα_2	0.220	31.9
Kβ_1	0.075	36.5
Kβ_2	0.024	37.4
Kβ_3	0.039	36.4
Kβ_4	<0.001	37.5
Kβ_5	<0.001	36.8
KO*	0.003	37.6
L	0.098	4.71
M	0.007	0.711
N	<0.001	0.123
Total	0.871	29.6
*All other K X-rays.		

231 **Table 3. X-ray average spectrum following ^{135}La decay.**

232 *Dosimetry*

233 The S-factors derived in this work are given in Table 4. From these results, it is clear that the calculated

234 cellular S-factors based on the BrIccEmis derived Auger spectrum of ^{135}La are different from those

235 obtained when using the spectrum from NuDat 2 [14]. The BrIccEmis derived spectrum yields higher

236 S(N←N) but lower S(N←Cy) and S(N←CS). These changes follow from the fact that the BrIccEmis

237 derived spectrum has a higher overall yield of low-energy Auger electrons and a slightly lower overall
238 yield of the higher-energy K-shell Auger electrons. The low-energy emissions are more dose-intensive
239 when inside the cell nucleus, while the higher energy emissions are more effective at supplying dose to
240 the nucleus when they are localized in cytoplasm and on cell surfaces. This is because low energy
241 emissions have a lower probability of reaching the nucleus from these compartments.

242 The S-factors calculated using the COOLER formalism show increased dose for the compartments (N←
243 Cy) and (N←CS), 38% and 89% respectively while (N←N) showed a 5% decrease, using this newly
244 calculated spectrum as compared to the MIRDCell formalism.

245

246 Comparing the dose delivered from ^{135}La to that of ^{177}Lu and ^{90}Y, it is seen that for (N←N), ^{135}La delivers
247 a higher dose to the nucleus than ^{177}Lu and ^{90}Y. However, this is not the case when the decay occurs in
248 the cytoplasm or on the cell surface. Comparing the new ^{135}La spectrum to ^{177}Lu, the dose ratio is 4 and
249 5.5 for the compartments (N←Cy) and (N←CS) respectively. This means that four disintegrations of
250 ^{135}La are needed to deliver absorbed dose, equal to that associated with a single disintegration of ^{177}Lu in
251 the cytoplasm. For ^{90}Y the dose ratios are 1.3 and 2, respectively. However, the number of interest when
252 assessing the potential of a therapeutic isotope is not the dose delivered per disintegration, but the target-
253 to-normal ratio i.e., the dose delivered to the target divided by the dose delivered to normal tissue.

254

	MIRDCell		COOLER	
S-value	BrIccEmis	NuDat 2 spectrum	BrIccEmis	NuDat 2 spectrum
S(N←N)	1.29E-03	9.51E-04	1.23E-03	9.45E-04
S(N←Cy)	6.81E-05	7.06E-05	9.39E-05	1.02E-04
S(N←CS)	3.09E-05	3.46E-05	5.84E-05	6.41E-05

255 **Table 4: Comparison of the cellular S-factors [Gy/(Bq*s)] for ^{135}La calculated in MIRDCell (left) and COOLER (right) using the**
256 **new Monte Carlo based Auger spectrum and, as reference, the input spectrum available in the NuDat 2 database** [14]**.**

257

	COOLER	MIRDCell	
S-value	^{135}La BrIccEmis	^{177}Lu MIRD	^{90}Y MIRD
S(N←N)	1.23E-03	1.05E-03	2.54E-04
S(N←Cy)	9.39E-05	2.78E-04	9.09E-05
S(N←CS)	5.84E-05	1.72E-04	6.15E-05

258 **Table 5 A comparison of the cellular S-factor [Gy/(Bq*s)] of ^{135}La calculated in COOLER, to those of the traditional β-emitting**
259 **therapeutic radionuclides ^{177}Lu and ^{90}Y calculated in MIRDCell.**

260 The relative merit of ^{135}La for single cell or small cell-cluster therapy as compared with the "standard"

261 therapeutic nuclides ^{177}Lu and ^{90}Y is obvious in Figure 3. It shows the fraction of emitted electron energy

262 absorbed within spheres of ever growing radii. Only ^{135}La is treated using both the COOLER and the Cole

263 stopping power approach, seeing that the COOLER formalism, at present, is not capable of handling the

264 high electron energies associated with ^{177}Lu and ^{90}Y decay (currently limited to 50 keV).
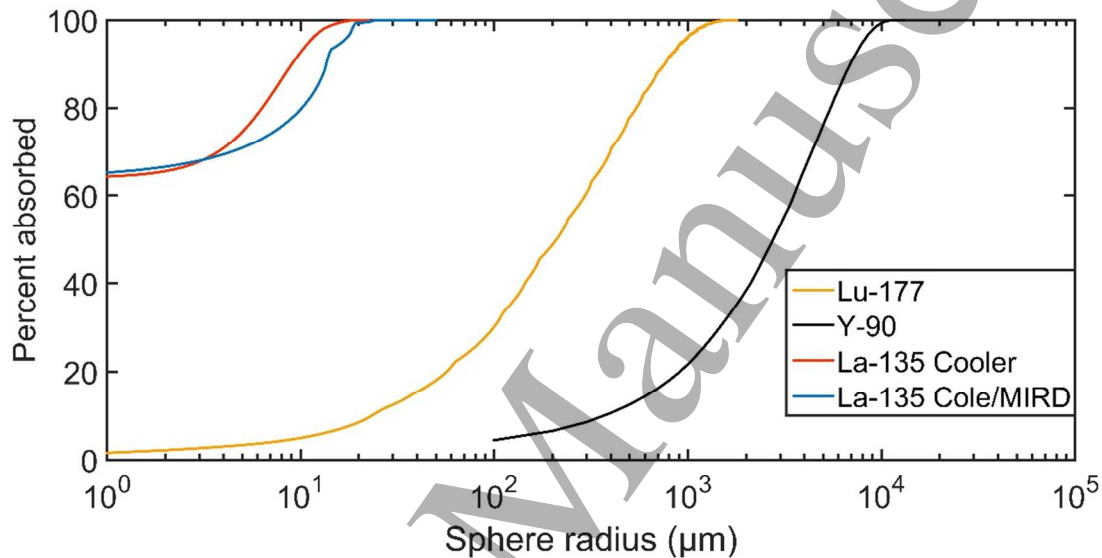
265

266 **Figure 3 Fraction of electron kinetic energy absorbed within spheres as function of sphere radius. The energy deposition is**
267 **calculated using the Cole stopping power as stated and used in the introduction of MIRD Cellular S-values [24], with**
268 **exception of the "La-135 Cooler" curve (red) which was calculated using the COOLER code. The input for the continuous**
269 **beta spectra are taken from RADAR[29] (^{90}Y and ^{177}Lu), the conversion- and Auger electrons from NuDat 2, except for**
270 **^{135}La, where the new, calculated Auger spectrum is used. Photons, including bremsstrahlung, are omitted.**

271 Figure 3 however, hides the full impact of the Auger emissions from ^{135}La. In very small spheres (radius

272 less than the diameter of cell nucleus) surrounding a ^{135}La decay, the local dose is very high. This can be

273 seen in Figure 4 which shows the dose-point kernel for ^{135}La as calculated with the new spectrum and

274 both the COOLER and the Cole stopping power formalisms.

275
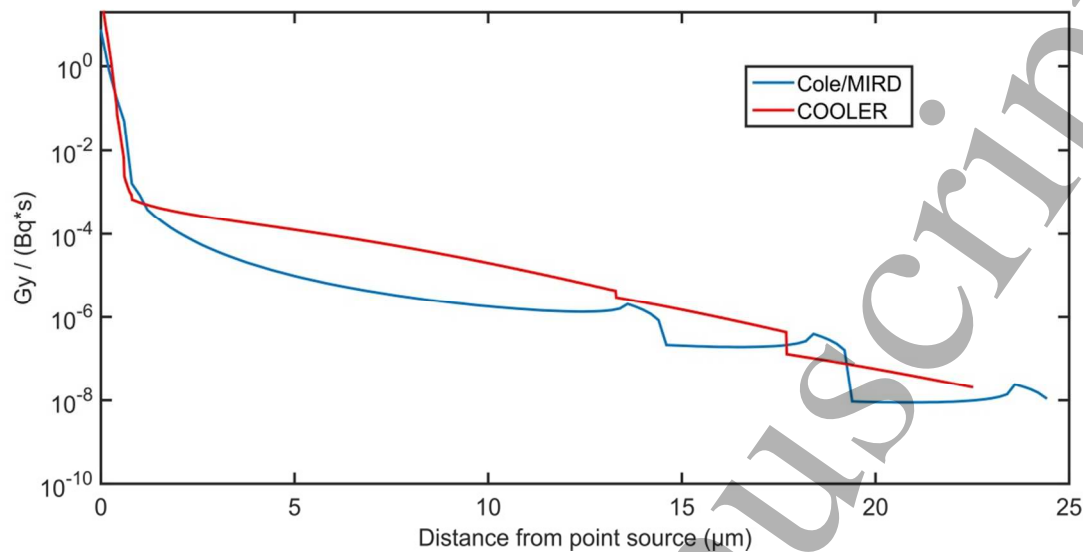
276

277 **Figure 4: Dose-point kernels for ^{135}La Auger electron emissions (X-rays are not included) for both the COOLER and**
278 **Cole/MIRD methodologies. In both cases, the calculations were performed using the Auger spectrum obtained from the**
279 **BrIccEmis simulation.**

280

281 **Discussion:**

282

283 The Auger emitter ^{135}La is a potential radionuclide for targeted internal therapy. From the view of

284 production and purification, the route via proton irradiation of ^{nat}Ba is straightforward. Clearly, the rate of

285 production and the radionuclidic purity of ^{135}La could be improved by irradiating enriched ^{135}Ba, but

286 further target development would be required to allow either irradiation of a barium oxide or salt, or to

287 accommodate reduction of recycled ^{135}Ba^{2+} after the separation procedure. While the overall separation

288 factor achieved in this report is not impressive $\sim 10^2$, the fact that high labeling effective specific activity

289 is obtained demonstrates that rigorous separation is not critical. Here, the measured effective specific

290 activity is a positive indicator for the expected labeling yield. The value measured by DTPA titration of

291 $(70.4 \pm 20.0 \text{ GBq/}\mu\text{mol})$ corresponds well with what would be expected from the ICP analysis. If, for

292 some applications, higher effective specific activities are required, an additional step to ensure the

293 removal of iron and manganese could be employed [30]. It should be noted that the exact impurity profile

294 of competing metals will depend on the initial purity of the barium stock used.

295

296 When turning to the emissions of ^{135}La, we show the results of calculations using the BrIccEmis code

297 from Lee et al. [16]. Importantly this method accounts for multiple vacancies during the cascade. Notably,

298 if the atomic transition energies are approximated using neutral binding energies, and thereby neglecting

299 the effect of multiple vacancies, this could give rise to multiple energies for a given atomic transition due

300   to the stochastic nature of the Auger cascade. Falzone & Lee et al. showed that MIRD RADTABS
301   disagree with the experimental L-Auger spectrum of [131]Cs and demonstrated that the theoretical L-Auger
302   energy spectrum of [131]Cs agreed with experiment only when the effect of multiple vacancies was taken
303   into account [27,31] .

304

305   In the present case, the use of the newly calculated Auger spectrum does not result in dramatically
306   different cellular dosimetry. However, the exact shape of the spectrum at low energies can become
307   extremely important as cellular and subcellular targeting becomes more exact. This is because the
308   expected biological effect of Auger emitters may not solely rely on the dose, but also on the RBE of the
309   low energy electrons. An important part of the Auger emitter concept is the expectation of an RBE larger
310   than that of conventional gamma or beta irradiation. RBE is the measure used to compare different types
311   of radiation gray-to-gray, assessing the biological damage done. A common measure for the biological
312   damage is DNA double-strand breaks, which are potentially more likely to occur in close proximity to the
313   decay site of an Auger emitter. For higher energy electron and beta emissions (> 20 keV), creating a
314   double-strand break with a single pass of an electron is highly unlikely because the mean path length
315   between subsequent ionization events is much larger than the distance between the DNA strands.
316   Therefore multiple electrons stemming from multiple decays have to pass through or get in close
317   proximity to the same area of the DNA strand to create a double-strand break. With an Auger emitter this
318   is not the case. Due to the multiple electrons emitted in a single decay (10.9 ± 3.2/decay for [135]La) only a
319   single decay is potentially enough to cause the double-strand break if the decay occurs close to the DNA.
320   Additionally, the decaying atom would find itself highly ionized due to multiple emissions of Auger
321   electrons and thus could be highly oxidizing to the immediate environment. From a physical perspective,
322   these two factors combined should result in an RBE much higher than 1, meaning more effective therapy
323   per gray deposited. A recent paper has described how the cell surface is more radiosensitive than assumed
324   in MIRD [32]. The calculations presented in this paper only consider dose to the nucleus, however
325   incorporating the cell surface as a sensitive target would make the case for [135]La even stronger, seeing that
326   this would decrease the importance of internalization.

327

328   It is also important to understand that the low amount energy emitted per decay of [135]La does not preclude
329   effective therapy. For therapeutic benefit, the relevant metric is not the absolute dose-per-decay but the
330   ratio of the dose absorbed by the target to the dose absorbed by the surrounding healthy tissue.
331   Commonly, the limiting factor is the absorbed dose in healthy tissue immediately surrounding the
332   targeted cell, or the absorbed dose in clearance organs. When considering the absorbed dose to the
333   immediate surroundings, the benefit of using [135]La is clear from Figure 3 and Figure 4, where the absence

334 of higher energy beta electrons and the limited Auger-electron range of ^{135}La results in dramatically

335 reduced dose beyond one cell diameter. As is the case with any Auger emitter, there are clear benefits of

336 using ^{135}La when the target being treated is very small.

337

338 **Conclusion:**

339 A method has been developed allowing the production of clinically relevant amounts of ^{135}La using

340 medical cyclotrons. The developed purification method is fast, robust and essentially loss-less. ^{135}La has a

341 well-suited half-life for therapy. The calculated cellular dosimetry shows that the emissions from ^{135}La

342 lead to cellular S-values that are promising for internal radionuclide therapy of very small targets, with

343 dosimetry superior to ^{177}Lu and ^{90}Y at single-cell dimension. This along with the mounting evidence of

344 Auger emitters having an RBE > 1 strongly motivates further research in application of Auger emitters in

345 treatment of single cancerous cells and micro-metastasis.

346

347 **Acknowledgements:**

348

351

352 **References**

353 [1]   Pfeifer AK, Gregersen T, Grønbæk H, Hansen CP, Müller-Brand J, Herskind Bruun K, et al.

354   Peptide receptor radionuclide therapy with 90Y-DOTATOC and 177Lu-DOTATOC in advanced

355   neuroendocrine tumors: Results from a Danish cohort treated in Switzerland. Neuroendocrinology

356   2011;93:189–96. doi:10.1159/000324096.

357 [2]   de Jong M. Combination Radionuclide Therapy Using 177Lu- and 90Y-Labeled Somatostatin

358   Analogs. J Nucl Med 2005;46:13–7.

359 [3]   Müller C, Reber J, Haller S, Dorrer H, Köster U, Johnston K, et al. Folate receptor targeted alpha-

360   therapy using terbium-149. Pharmaceuticals 2014;7:353–65. doi:10.3390/ph7030353.

361 [4]   Müller C, Reber J, Haller S, Dorrer H, Bernhardt P, Zhernosekov K, et al. Direct in vitro and in

362   vivo comparison of 161Tb and 177Lu using a tumour-targeting folate conjugate. Eur J Nucl Med

363   Mol Imaging 2014;41:476–85. doi:10.1007/s00259-013-2563-z.

364 [5]   Müller C, Zhernosekov K, Köster U, Johnston K, Dorrer H, Hohn A, et al. A unique matched

365   quadruplet of terbium radioisotopes for PET and SPECT and for α- and β- radionuclide therapy:

366   an in vivo proof-of-concept study with a new receptor-targeted folate derivative. J Nucl Med

367   2012;53:1951–9. doi:10.2967/jnumed.112.107540.

368   [6]   Grünberg J, Lindenblatt D, Dorrer H, Cohrs S, Zhernosekov K, Köster U, et al. Anti-L1CAM
369   radioimmunotherapy is more effective with the radiolanthanide terbium-161 compared to
370   lutetium-177 in an ovarian cancer model. Eur J Nucl Med Mol Imaging 2014;41:1907–15.
371   doi:10.1007/s00259-014-2798-3.

372   [7]   Kassis AI. Molecular and cellular radiobiological effects of Auger emitting radionuclides. Radiat
373   Prot Dosimetry 2011;143:241–7. doi:10.1093/rpd/ncq385.

374   [8]   Howell RW, Kassis AI, Adelstein SJ, Rao D V, Wright HA, Hamm RN, et al. Radiotoxicity of
375   platinum-195m-labeled trans-platinum (II) in mammalian cells. Radiat Res 1994;140:55–62.
376   doi:10.2307/3578568.

377   [9]   Azure MT, Sastry KSR, Archer RD, Howell RW, Rao D V. Microscale Synthesis of Carboplatin
378   Labels with the Auger Emitter Platinum-193m: Radiotoxicity Versus Chemotoxicity og the
379   Antitumor Drug in Mammalian Cells. AAPM Symp. Ser. No.8, 1992.

380   [10]   Kassis AI. Cancer therapy with Auger electrons: are we almost there? J Nucl Med 2003;44:1479–
381   81.

382   [11]   Abel EP, Clause HK, Fonslet J, Nickles RJ, Severin GW. The Half-lives of 132La and 135La.
383   arXiv.org 2017:1–11.

384   [12]   Fonslet J, Tran T, Quan-Lee B, Severin G. 135La for Auger-based therapy: preparation, imaging
385   and emissions. J Label Compd Radiopharm 2015;58:S24.

386   [13]   Singh B, Rodionov AA, Khazov YL. Nuclear Data Sheets for A = 135. Nucl Data Sheets
387   2008;109:517–698. doi:10.1016/j.nds.2008.02.001.

388   [14]   Nudat 2 n.d. http://www.nndc.bnl.gov/nudat2/ (accessed May 30, 2017).

389   [15]   Lee BQ, Kibédi T, Stuchbery E, Robertson K. Atomic radiations in the decay of medical
390   radioisotopes: a physics perspective. Comput Math Methods Med 2012;2012:651475.
391   doi:10.1155/2012/651475.

392   [16]   Lee BQ, Nikjoo H, Ekman J, Jönsson P, Stuchbery AE, Kibédi T. A stochastic cascade model for
393   Auger-electron emitting radionuclides. Int J Radiat Biol 2016;92:641–53.
394   doi:10.3109/09553002.2016.1153810.

395   [17]   Prescher K, Peiffer F, Stueck R, Michel R, Bodemann R, Rao MN, et al. Thin-target cross sections
396   of proton-induced reactions on barium and solar cosmic ray production rates of xenon-isotopes in
397   lunar surface materials. Nucl Inst Methods Phys Res B 1991;53:105–21. doi:10.1016/0168-

398   583X(91)95645-T.

399   [18]   Tárkányi F, Ditrói F, Király B, Takács S, Hermanne A, Yamazaki H, et al. Study of activation

400   cross sections of proton induced reactions on barium: Production of 131Ba 131Cs. Appl Radiat

401   Isot 2010;68:1869–77. doi:10.1016/j.apradiso.2010.03.010.

402   [19]   Severin GW, Gagnon K, Engle JW, Valdovinos HF, Barnhart TE, Nickles RJ. 44gSc from metal

403   calcium targets for PET. AIP Conf Proc 2012;1509:125–8. doi:10.1063/1.4773953.

404   [20]   Vaziri B, Wu H, Dhawan AP, Du P, Howell RW. MIRD pamphlet No. 25: MIRDcell V2.0

405   software tool for dosimetric analysis of biologic response of multicellular populations. J Nucl Med

406   2014;55:1557–64. doi:10.2967/jnumed.113.131037.

407   [21]   Goddu SM, Howell RW, Rao D V. Cellular dosimetry: absorbed fractions for monoenergetic

408   electron and alpha particle sources and S-values for radionuclides uniformly distributed in

409   different cell compartments. J Nucl Med 1994;35:303–16.

410   [22]   Siragusa M, Baiocco G, Fredericia PM, Friedland W, Groesser T, Ottolenghi A, et al. The

411   COOLER Code: A Novel Analytical Approach to Calculate Subcellular Energy Deposition by

412   Internal Electron Emitters. Radiat Res 2017;188:204–20. doi:10.1667/RR14683.1.

413   [23]   Friedland W, Dingfelder M, Kundrát P, Jacob P. Track structures, DNA targets and radiation

414   effects in the biophysical Monte Carlo simulation code PARTRAC. Mutat Res - Fundam Mol

415   Mech Mutagen 2011;711:28–40. doi:10.1016/j.mrfmmm.2011.01.003.

416   [24]   Cole A. Absorption of 20-eV to 50,000-eV Electron Beams in Air and Plastic. Radiat Res

417   1969;38:7. doi:10.2307/3572707.

418   [25]   Lee BQ, Kibédi T, Stuchbery AE. Auger yield calculations for medical radioisotopes. EPJ Web

419   Conf 2015;91:7. doi:10.1051/epjconf/20159100007.

420   [26]   Khazov Y, Rodionov A, Kondev FG. Nuclear Data Sheets for A = 133. Nucl Data Sheets

421   2011;112:855–1113. doi:10.1016/j.nds.2011.03.001.

422   [27]   Falzone N, Lee BQ, Fernandez-Varea JM, Kartsonaki C, Stuchbery AE, Kibedi T, et al. Absorbed

423   dose evaluation of Auger electron-emitting radionuclides: impact of input decay spectra on dose

424   point kernels and S -values. Phys Med Biol 2017;62:2239–53. doi:10.1088/1361-6560/aa5aa4.

425   [28]   Emfietzoglou D, Nikjoo H. Accurate electron inelastic cross sections and stopping powers for

426   liquid water over the 0.1-10 keV range based on an improved dielectric description of the Bethe

427   surface. Radiat Res 2007;167:110–20. doi:10.1667/RR0551.1.

428   [29]   RADAR Home n.d. http://www.doseinfo-radar.com/RADARHome.html (accessed May 30, 2017).

429   [30]   Fonslet J, Tietze S, Jensen AI, Graves SA, Severin GW. Optimized procedures for manganese-52:

430   Production, separation and radiolabeling. Appl Radiat Isot 2017;121:38–43.

431   doi:10.1016/j.apradiso.2016.11.021.

432   [31]   Eckerman KF, Endo A. MIRD: radionuclide date and decay schemes. Society of Nuclear

433   Medicine; 2008.

434   [32]   Paillas S, Ladjohounlou R, Lozza C, Pichard A, Boudousq V, Jarlier M, et al. Localized

435   Irradiation of Cell Membrane by Auger Electrons Is Cytotoxic Through Oxidative Stress-Mediated

436   Nontargeted Effects. Antioxid Redox Signal 2016;25:467–84. doi:10.1089/ars.2015.6309.

437